SEDIMENTOLOGY the journal of the International Association of Sedimentologists

Sedimentology (2020) **67**, 2747–2763 doi: 10.1111/sed.12718

Geobiological model of ripple genesis and preservation in a heterolithic sedimentary sequence for a supratidal area

DIANA G. CUADRADO*†

*Instituto Argentino de Oceanografía (IADO), UNS-CONICET, Florida 7500, Bahía Blanca 8000, Argentina (E-mail: cuadrado@criba.edu.ar)

†Dpto. de Geología, Universidad Nacional del Sur (UNS), Av. Alem 1253, Cuerpo B. 2° Piso, Bahía Blanca 8000, Argentina

Associate Editor – Jaco Baas

ABSTRACT

This study documents the processes involved in forming flaser and wavy bedding governed by microbial activity in sediments. It focuses on a modern marginal-tidal system providing evidence of the role that biofilms play in the stabilization of ripples and their potential preservation. A combination of detailed field work, analysis of water level records and microscopic petrographic inspection were used to reply to the question: how fine-grained and coarse-grained sediments can sequentially be deposited and preserved in a coastal environment. The hydraulic energy was measured by water level sensors recording flooding events that inundate the colonized tidal flat. Changing surface morphologies were monitored after storms, revealing the importance of biological processes in the preservation of ripples. A mud drape over ripples was observed several days after the undulated surface formation, known as a sinoidal sedimentary structure, which is a thin biofilm covering the ripples, caused by the presence of a microbial mat. Because bedforms are essential predictors of palaeoenvironmental reconstruction, interpretation in the geological record should take into consideration the important effect that colonized sediments have on the preservation of ripples. A geobiological model explains the flaser sedimentation, common in depositional coastal environments, suggesting that the hydrodynamic conditions may not be directly reflected by the grain size at the time of deposition. The study reveals that flaser sedimentation involves an interaction with benthic organisms, reflected by the sequence of microbial mats with sand ripple marks. A detailed description of heterolithic sequences shows that the presence of microbial activity can drive ripple preservation. This suggests that hydraulic interpretation of the sedimentary record based only on physical processes might be erroneous.

Keywords Flaser bedding, microbial mat, MISS, mud drape, sinoidal structures, tidal flat.

INTRODUCTION

Flaser bedding is common in tidal flat environments (Reineck & Wunderlich, 1968) and is usually interpreted as a product of the alternation of current or wave action and subsequent slack water, considered as a combination of more and less energetic conditions (Davies, 2012). However, the thickness of the mud drape does not exceed a few millimetres and there is a sharp boundary between mud and sand, and the mud is fairly homogeneous (Terwindt & Breusers, 1982). Besides, the preservation potential of wavy bedding requires a rapid consolidation after

deposition to decrease the possibility of the next flood removing this fine sediment layer (Martin, 2000). In this regard, Neumann *et al.* (1970) demonstrated the biostabilizing properties of microbenthic communities and documented their erosion resistance. The term 'biostabilization' was introduced by Paterson (1994) to account for the increase in the critical erosion threshold for the resuspension of particles by bacterial activities that protect the seafloor deposits against erosional processes increasing the preservation potential of sedimentation (Gehling, 1999). Biostabilization also includes the sealing of the surface by EPS (Extracellular Polymeric Substances) secreted by micro-organisms (Noffke *et al.*, 2001).

Recent studies highlighted the organic factor in sedimentary processes, such as heterolithic sequences formed by fine grains (silt and clay) in sands, that were explained by the interaction of biological processes under strong hydrodynamic conditions (Cuadrado *et al.*, 2014; Wooldridge *et al.*, 2017; Virolle *et al.*, 2018). The microbial presence in sediments changes the response to hydrodynamic conditions; therefore, the energy is not directly reflected by the grain size at the time of deposition. Hence, identification of biological activity is important in the interpretation of the sedimentary record, because sedimentation is closely connected with biological activity, and the organic layers produced by microbial activity can be misinterpreted as less energetic sedimentation (Cuadrado & Blasi, 2017).

Heterolithic bedding is considered an excellent tidal signature of many intertidal and subtidal environments, but also in estuaries and the interdistributaries of deltas (Dalrymple *et al.*, 2012; Davies, 2012; Steel *et al.*, 2012; Wang, 2012). They may also form in fluvial environments but their cyclicity suggests a tidal phenomenon (Davies, 2012). However, this paper shows examples from a supratidal flat colonized by microbial mats. In tidal flat settings rich in biofilms, biostabilization by EPS plays a key role in binding of fine-grained particles and sand grains (Eisma, 1986). The present study documents heterolithic sedimentation governed by microbial colonization in a modern marginal-tidal system, providing evidence of the role that biofilms play in the stabilization of ripples immediately after their formation. The hypothesis of the study is that mud drapes covering ripple marks are not directly related to physical processes. Mud drapes are conventionally interpreted as indicating low-energy deposition, but this study demonstrates that they are formed by microbial activity in a more energetic environment when the bed is immobilized by a mat. They are created by the interaction between sediment and micro-organisms.

This study was carried out in the supratidal flats in Paso Seco (Argentina), characterized by a strong, erosion-resistant microbial mat, which persists even under intermittent high-energy hydrodynamic events (Cuadrado & Pan, 2018; Maisano *et al.*, 2019). The study documents how the ripple marks created during storms become stabilized by microbial activity that starts colonizing the fresh deposits, so that a flaser bedding is developed.

STUDY AREA

Paso Seco (40°38′4″S; 62°12′22″W; Fig. 1) is a mesotidal coastal environment, where mean and maximum tidal ranges are 1.62 m and 2.5 m, respectively. It is a continental to shallow marine transitional environment comprising an elongated area (>3 km in length) behind a sand spit generated by longshore sediment transport that closed off a tidal channel. The evolution of the sand spit included two phases of seaward coastal progradation (phases 'I' and 'II' in Fig. 1; Trebino, 1987). A semi-closed area behind the barrier is categorized as a supratidal zone because it is flooded by seawater only during storms that may occur up to 43 times per year, but remains unaffected by daily flood tides (details in Maisano *et al.*, 2019; Perillo *et al.*, 2019). This alternation between quiescence and flooding events provides optimal conditions for an epibenthic microbial mat to form (Noffke, 2010), which covers a wide area of *ca* 1.8 km^2 in size. The main constructor of these epibenthic microbial mats is the cyanobacteria *Microcoleus chthonoplastes*, a cosmopolitan species that forms thick bundles enclosing several individual trichomes with a polysaccharide sheath (Stal, 2003). The cyanobacteria are embedded within the matrix of their EPS that give a leathery structure and stability to the mat. The mat comprises associated diatoms, mostly pennates (Cuadrado & Pan, 2018), as a thin sheet that can be seen as a brownish layer on the top of many tidal sediments (Stal, 2013).

The episodic inundation of the area displays hydrodynamic conditions characterized by a fast flood and slow ebb. These characteristics are enhanced by the coastal geomorphology of the confined and elongated tidal flat (Maisano *et al.*, 2019; Perillo *et al.*, 2019). The narrowing

Fig. 1. Location of Paso Seco tidal flat, behind the sand spit (Phases I and II of formation after Trebino, 1987). The study area colonized by microbial mats is contoured.

produces a current amplification and the water column reaches a maximum of 78 cm over the colonized flat. The fast flood currents are the primary factor in developing large microbial deformation structures such as roll-ups and folds, several metres in size (Cuadrado *et al.*, 2015; Maisano *et al.*, 2019). These huge structures form simultaneously with ripples during a storm.

METHODS

Inundation of the microbial flat was recorded by a water level logger (HOBO by Onset-model U20; 2.5 cm diameter and 15 cm length; Onset Computer Corporation, Bourne, MA, USA) from May 2015 to December 2018, and discontinued only during Austral summers (December to March 2015–2016 and 2017–2018). The logger was deployed in a vertically buried, perforated PVC pipe, 40 cm in length, and recorded the pressure (water plus atmospheric) and water temperature every 10 min. These data were corrected by atmospheric pressure, measured by another logger placed on an upper surface, to obtain only water depth data. The sensor data were collected during the three months and five months of field work. The microbial mat development was monitored by photography during each visit of the site. Sedimentary cores were obtained using PVC tubes (3.5 cm diameter and 20 cm length), and sedimentary blocks with a surface of 4×10 cm and 8 cm depth were extracted from the tidal flat to examine the sedimentary texture and granulometry. In the laboratory, the cores were opened up, so that the sediment dried somewhat, which allowed the lamination to become more clearly visible. Sediment grain size was determined with a laser diffraction particle analyzer Malvern Mastersizer 2000 (Malvern Panalytical Limited, Malvern, UK).

RESULTS

Sedimentary characteristics of a sequence in a mat-covered area

The cores exhibit sand and mud alternation in a heterolithic sequence (Fig. 2A). The scale of these rhythmic packages ranges from a few millimetres to several centimetres. The contact between laminae is sharp, planar and paralleled (Fig. 2A); however, sometimes the contact is undulating or wavy. Also deformation structures can be noticed (star symbol in Fig. 2B). Laminae can reach up to 7 cm in thickness (Fig. 2A), which are then called layers. The sand laminae (or layers) are dominated by very fine or fine sand with opaque minerals. The thicker sand layers include sponge pore fabrics, a secondary high porosity typical for sand intercalated between two buried mat layers caused by gases derived from bacterial metabolic activity (Noffke, 2010). The sedimentary core is always capped by >1 cm thick microbial mats (Fig. 2A). When the sedimentary core becomes dried out it breaks up slightly along sand layers (white

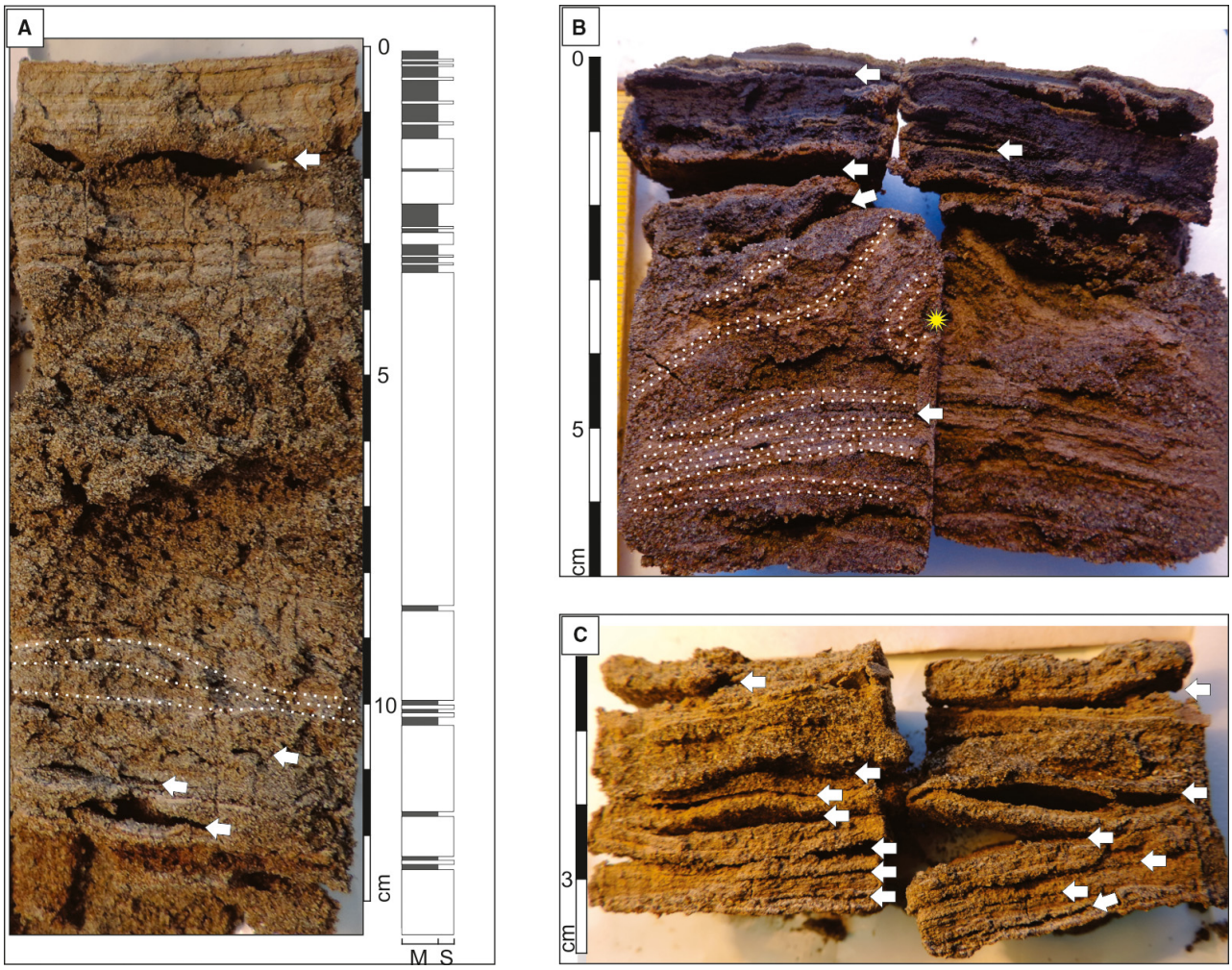

Fig. 2. Sediment cores. (A) Biolaminite showing the alternation of microbial mats (S = fine sand; M = mud in the sedimentary log). Dense microbial mats are present on the top. (B) Planar microbial mats at the base of the core anoxic mats are present in the top 1 cm. A characteristic deformation structure is shown by a star. (C) Disintegration of a dried core along sand layers. White arrows show sand layers where the core disintegrated.

arrows in Fig. 2A and C); conversely, the mud layers remained tightly maintained.

General hydrodynamic regime

The microbial flat is flooded by the sea several times a year during frequent storm events of different energy levels. In the period between November 2016 and October 2017 (Fig. 3A), the seawater flooded the area 28 times; on 11 occasions the water column exceeded 20 cm, and on one occasion it exceeded 40 cm as a consequence of a severe storm (May 2017). In four years there were only five severe storms, when the water column in the study area exceeded 40 cm.

There is a clear difference in the fluctuation of the water level between winter and summer. In Austral winter (May to August, rectangle in Fig. 3A) the water table remains near the surface for more than a month, whilst in summer the water level varies considerably below the sedimentary surface reaching more than 40 cm in depth. However, flooding events can occur at any time throughout the year. In fact, in Austral summer (December 2016), the highest water column over the microbial flat was 45 cm. All flooding events show a similar pattern in the study area: the flood currents are fast and short-lived and subsequent ebb currents are slow, draining the surface gradually.

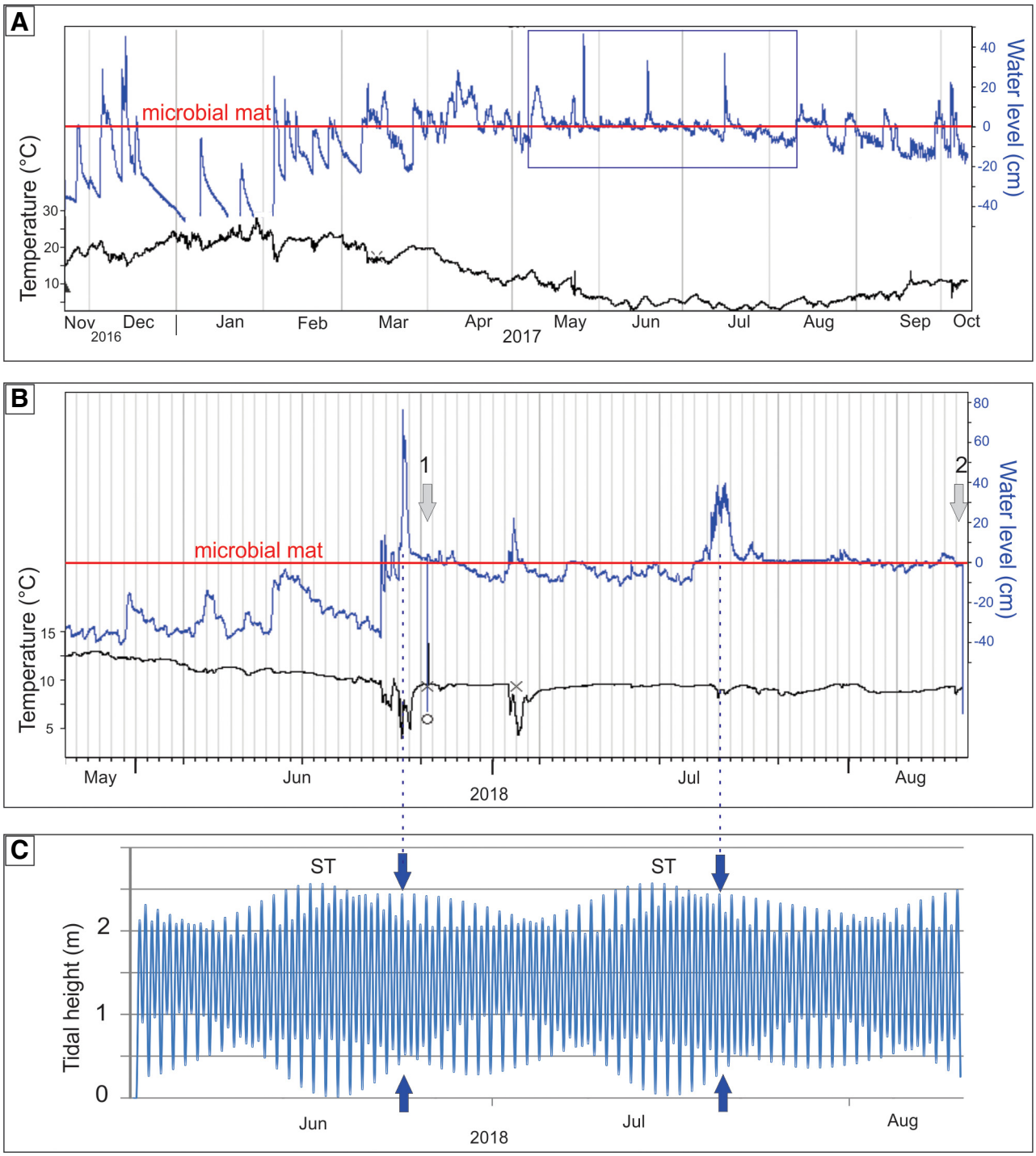

Fig. 3. (A) Yearly water level and temperature record. The level of water over the microbial mats shows the sea inundation during storms. (B) Severe storm recorded in June and July 2018. Field trips were indicated by arrows 1 and 2. (C) Predicted tides. The arrows indicate the high and low tide for the high inundation in (B). ST, spring tide.

The largest flooding event over the microbial flat since 2015 was due to a storm characterized by strong winds (*ca* 50 km h^{-1} south-west direction, calculated by Global Forecast System by NOAA, with resolution of 27 km) during several days in Austral winter 2018 (June, Fig. 3B).

This event resulted in significant wave heights up to *ca* 4 m (deep-water values obtained by NWW3 wave forecast model by NOAA with resolution of 50 km). The predicted high tide when the severe storm occurred was 2.44 m, close to spring tide value of 2.54 m. The corresponding low tides were also high (0.52 m; arrows in Fig. 3C). These meteorological and oceanographic conditions caused the inundation of the study area, with the water column rising up to a maximum 78 cm (Fig. 3B). Two days after the largest inundation, a field survey was carried out (arrow 1 in Fig. 3B), when a shallow 5 cm sheet of water was covering the tidal flat.

The subsequent large flood that occurred in mid-July 2018 caused the water column to reach a height of 40 cm after two days of continuous winds >50 km h^{-1} blowing from the south and south-east inducing significant wave heights >4 m. Similar to the preceding severe event, the predicted high tide (2.44 m) was close to spring tide value with correspondingly high low tides (0.58 m; Fig. 3C). The high seawater level near spring tide was reinforced by strong winds in the study area. After the flooding event, the seawater was maintained on the microbial mat for more than 10 days (Fig. 3B), and a field trip was carried out 20 days after this large flooding event (arrow 2 in Fig. 3B).

Sediment transport and rippled bed development

The large flood in June 2018 (arrow 1 in Fig. 3B) created erosional pockets and several mat deformation structures (details in Maisano *et al.*, 2019) due to the detachment of the microbial mat from the underlying sediment. Water currents deformed the mat into roll-ups, and flipped-over edges; microbial gas domes formed by gas migrating vertically through the sediment, most likely deriving from the gas-filled sponge pores beneath the microbial mat (Fig. 4A to C). The flood currents also caused sand transport across both the microbial mats and the exposed sediment (yellow arrows in Fig. 4A and B). Several types of ripples were created (Fig. 4D to F) among the erosional features. Asymmetrical two-dimensional and three-dimensional bedforms were formed by flood currents, with continuous wavy crestlines, wavelengths with a range of 5 to 10 cm and heights of about 1 cm. There is mud in the trough of the ripples which was deposited during less energetic conditions (white arrows in Fig. 4C to F). Ripples were deposited in a sharp and planar contact to the microbial mat beneath (MM, Fig. 4G and H). The body of the ripples is generally composed of fine sand, with very little thickness in the ripple troughs (arrow in Fig. 4G). The oxic brownish surficial layer of the microbial mat beneath the ripple displays a planar lamination, which is underlain by an anoxic layer. Very thin sand layers (1 to 2 mm) form part of the microbial mat (arrows in Fig. 4H).

During the field trip carried out in August 2018 patches of stabilized ripples were seen on the tidal flat (Fig. 5A). These ripples were formed due to the sediment transported during the storm in mid-July, 20 days before the field trip. The 2D and 3D asymmetrical and symmetrical ripples presented similar dimensions to those measured previously (wavelength *ca* 10 cm; height *ca* 1 cm, Fig. 5B to D) and mud was deposited in the troughs (arrows in Fig. 5B and D). Also, the detached microbial mat that formed folds and folded-over edges (Fig. 5E and F; for process formation see Maisano *et al.*, 2019) resulted in very small biostabilized ripples on its surface (wavelength *ca* 6 cm, height *ca* 1 to 2 mm). These small ripples are depositional features formed by accumulation of sand on the microbial mat (Fig. 5G and H), which are characterized by an oxic surficial layer over successive planar thin anoxic layers (Fig. 5G and H). Commonly, the sand layer presents oxic conditions *in situ* and the fine sediment layers in microbial mats below exhibit anoxic conditions (Fig. 6A and B). Over a few days, aerial exposure of the mud erased the anoxic appearance, and the microbial mats can only be distinguished by planar fine sediment centimetre or millimetre-scale laminations between sand layers (Fig. 6C).

Characteristics of the ripple marks on mat-colonized sediment

A vertical core of 8 cm depth, extracted from the microbially stabilized substrate after the storm, exhibits a discrete sand ripple (Fig. 7). The ripple surface is overlaid by a millimetre-sized mud drape and the sand ripple rests on the microbial mat (Fig. 7A). Underneath, towards the bottom, several planar sand sheets are capped by a biofilm (arrows in Fig. 7A), although they do not all show the same thickness. The sand in the ripple body shows a greenish colour due to the presence of green filamentous cyanobacteria (Fig. 7B to D).

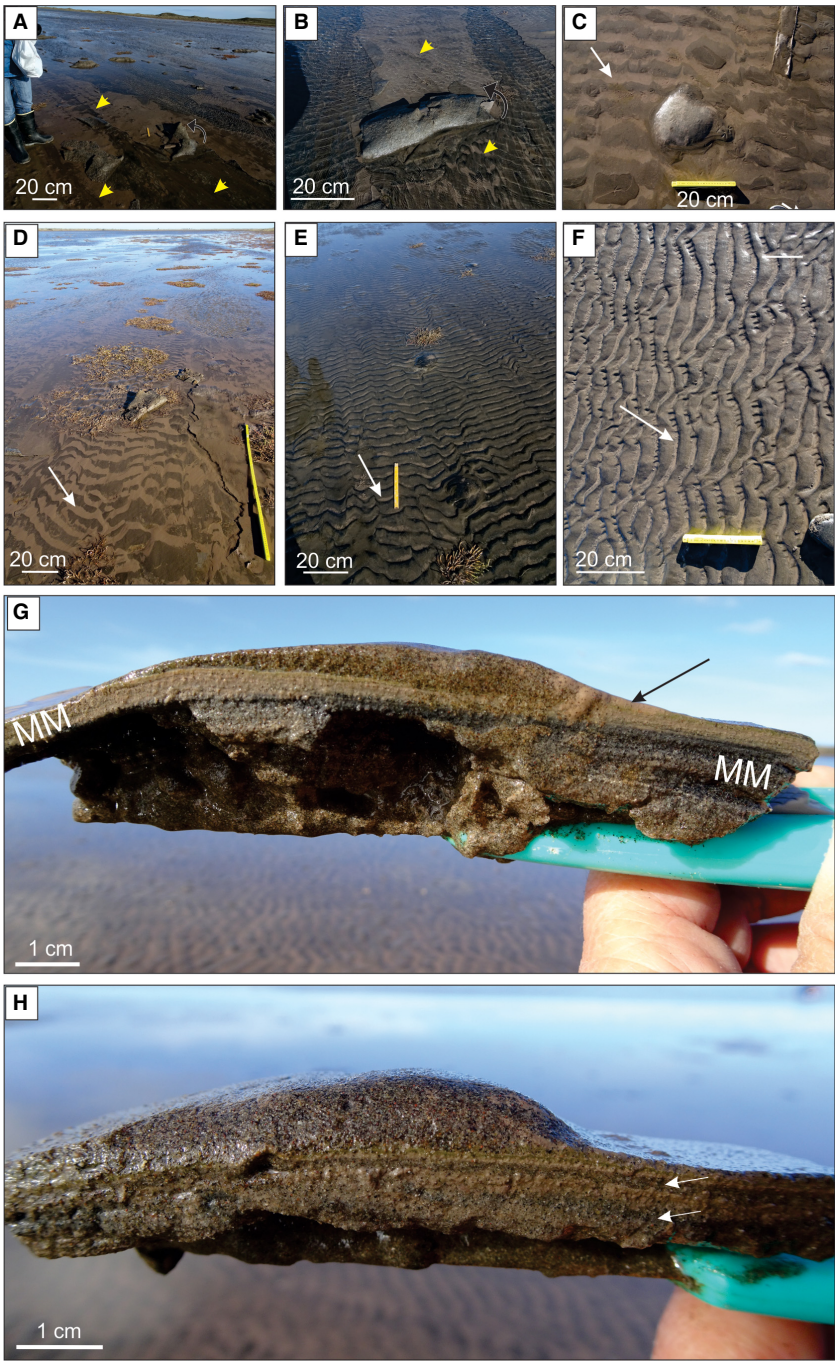

Fig. 4. Tidal flat appearance in the field trip carried out in June, two days after a severe storm. (A), (B) and (C) Deformed microbial structures: (A) detached piece of mat; (B) microbial roll-up; and (C) microbial gas dome. Curved arrow shows the direction of mat deformation by flood currents. The deformation structures were created in association with ripples (yellow arrows). (D), (E) and (F) Different ripple morphology created by the sediment transport. Fine sediment deposited in the trough of the ripples (white arrow). (G) and (H) Vertical section of a ripple showing the asymmetrical bedform deposited over the microbial mat laminae (MM) that consists in planar layers. Fine sediment is shown by an arrow in the trough of the ripple (G). The microbial mat presents two sand planar layers – white arrow in (H). For deformation processes see Maisano *et al.* (2019).

The filaments were among the quartz grains interweaving the sand particles in the uppermost few millimetres of the sedimentary surface. Eight millimetres beneath the surface, among planar and parallel microbial laminae of different width, there are also lee faces of a buried sand ripple (Fig. 7E). In contrast to the ripple on the surface of the core, a close-up view of the colonized sand shows translucent EPS strands interweaving the sediment particles (Fig. 7F).

In a vertical section of the tidal flat, heterolithic layers of millimetre thicknesses can be distinguished (Fig. 8A). Alternations of planar to rippled sand layers and draping mud indicate thin wavy bedding. At the bottom of the section a body of sand with millimetre-thick biofilms occurs, seen as interlayers of mud in undulating surfaces (Fig. 8A and B). A close-up of these thin mud layers exhibits the presence of EPS, which cause cohesion in the sediments (Fig. 8C). Throughout

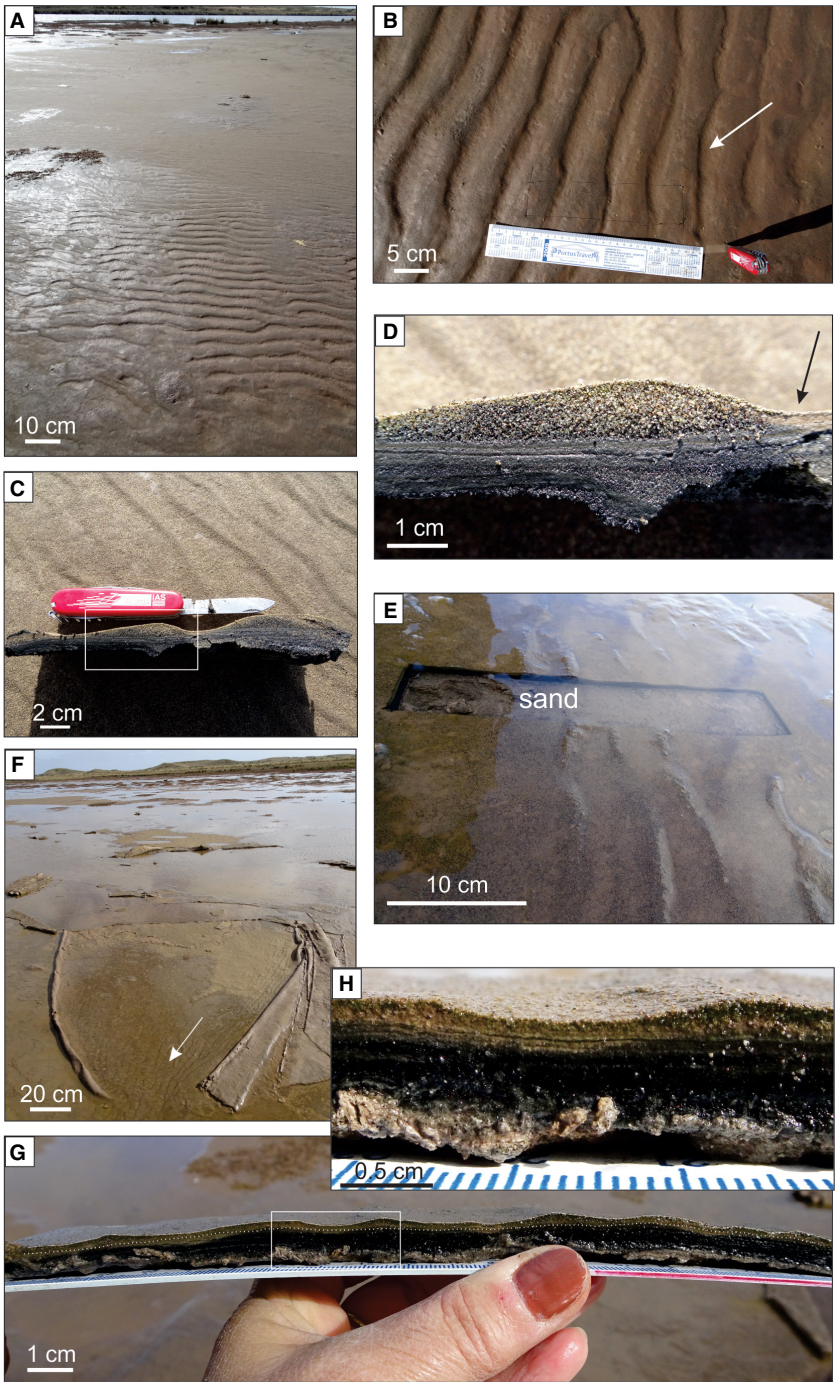

Fig. 5. Tidal flat appearance in the field trip carried out in August, 20 days after a severe storm. (A) Stabilized ripples on the microbial mat. (B) Details of the ripples with fine sediment deposited in the trough (white arrow). (C) A vertical section perpendicular to the crests extracted from the tidal flat. The sand ripple was formed over the planar microbial mat (anoxic). (D) Details of the sand ripple showing fine sediment in the trough (arrow). The geoform is covered by a thin biofilm. (E) The site where the vertical section was extracted from the microbial mat showing the oxic sand. (F) Association of mat fold structures with sand ripples over the mat. (G) View of the extracted vertical section extracted in (E). The dotted line indicates the surface of microbial mat where the sand ripples were deposited. (H) Close-up of (G). The mat shows an oxic layer at the top, and anoxic layer below, formed over oxic sand sediment.

the section, there are several planar layers of organic sediment, <1 to 2 mm thick (Fig. 8D) forming the lee face of a buried ripple towards the right side of the section (Fig. 8E). The close-up of the fine sediment shows green filaments of cyanobacteria remaining in the layer (Fig. 8F and G). Atop the section, sand is deposited over the planar fine layer (microbial mat laminae, thickness >2 mm) forming a ripple (Fig. 8H).

Microscopic analysis

Petrographic analyses of thin-sections show microscopic textures that exhibit fabric typical of microbial presence (Fig. 9). The finer grains and organic matter form a discrete sheet (microbial presence) that is laterally continuous and coats the layers of sand, which represent the former current velocity strength. Organic matter sheets are former biofilms, similar to those

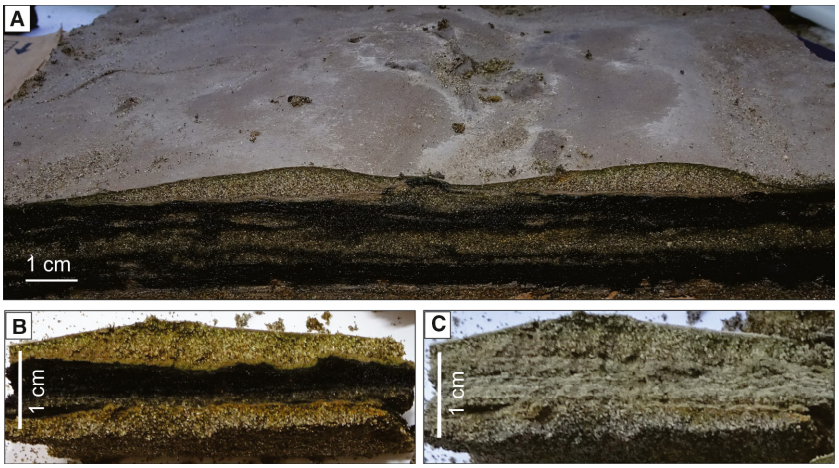

Fig. 6. *In situ* vertical section of a microbial mat. (A) Stabilized ripples at the surface, showing the anoxic fine sediment (microbial mat) and the oxic sand ripple at the top. (B) and (C) Comparison of the same section after several days. The anoxic condition disappeared and a fine sediment layer can be shown.

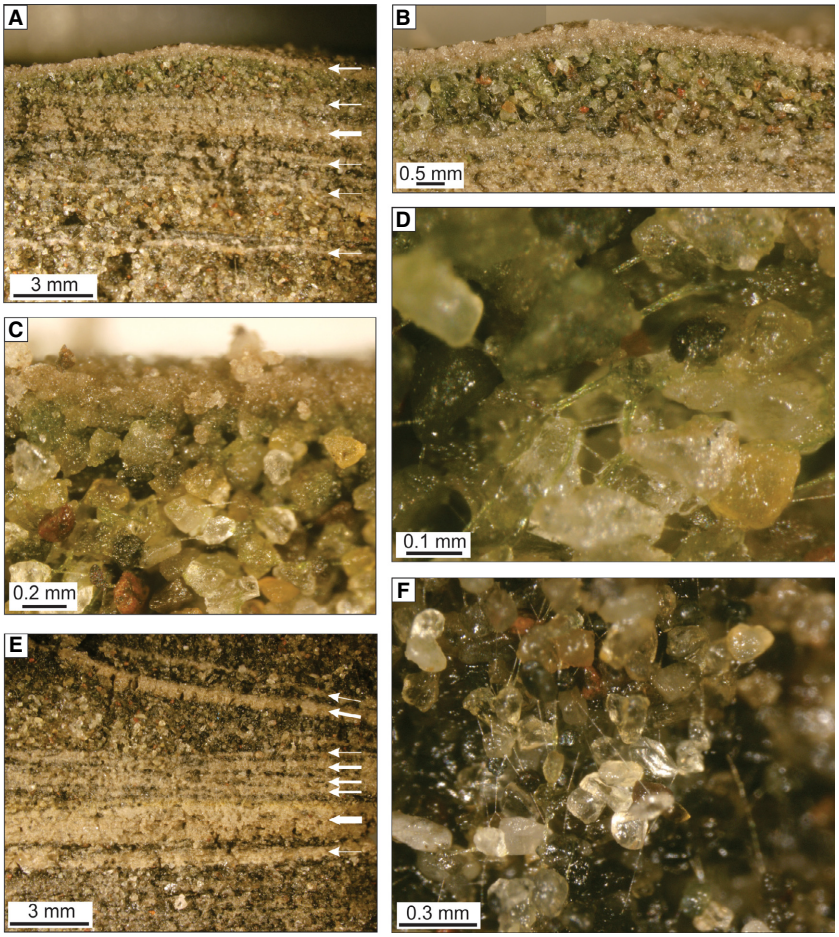

Fig. 7. Vertical stabilized ripple under optical microscope. (A) The sand ripple (2 mm height) over microbial mat composed of fine sediment layers of different thicknesses (arrows). (B) Close-up of (A). The sand body of the ripple has a greenish colour and is covered by a biofilm. (C) and (D) Close-up of the sand in the ripple (B). The sand grains are intertwined by green cyanobacteria filaments. (E) View of the bottom of the vertical section (A). A buried ripple was deposited over a planar microbial mat. The biofilm that covered the ripple is a sinoidal structure (Noffke, 2010). (F) Close-up of (E) where translucent EPS strands entangled sand grains.

observed on the ripple surface (Fig. 7B). The two uppermost sand laminae in Fig. 9A include randomly oriented grains of the largest grain size in the sample, still being transported by the current forming this deposit. All sand laminae were separated by biofilms or mat laminae visible as dense lines identified as organic matter or thin bacterial filaments. In Fig. 9B, the lower

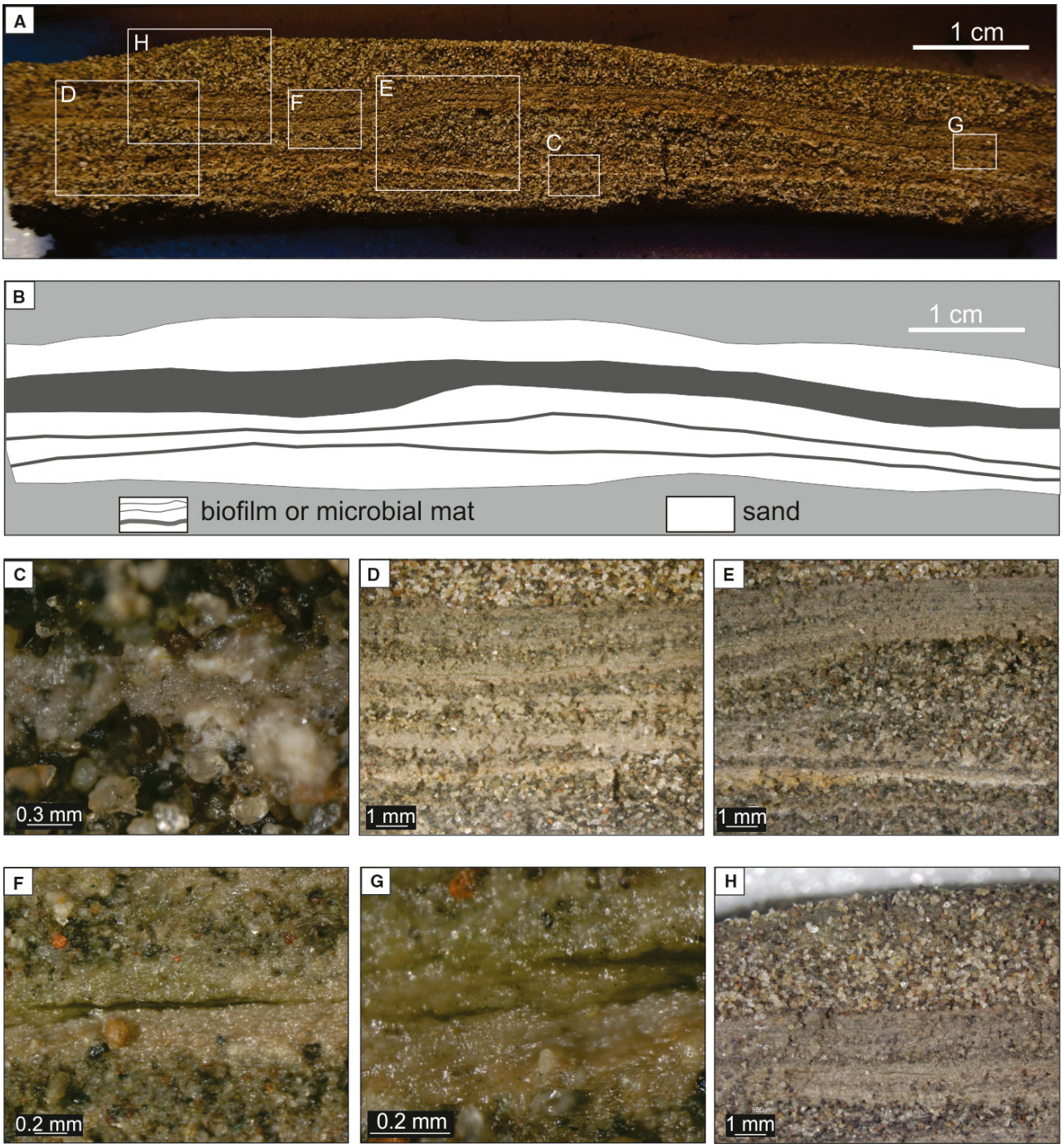

Fig. 8. Vertical stabilized sedimentary section. (A) Photograph of the section comprising undulating sand layers between microbial mat layers. (B) Schematic diagram of (A). (C) Close-up of EPS biofilm in a sinoidal structure at the bottom of the section. (D) Typical lamination of microbial mats. (E) Lee face of a ripple situated over a microbial mat (planar bottom lamination) and covered with mat. (F) and (G) Close-up of biofilm with the presence of filaments of cyanobacteria. (H) Sand ripple on the surface of the sedimentary section deposited over a microbial mat >1 mm.

planar organic sheets are parallel in contrast to the upper one covering a ripple lee face. Also, thicker organic matter (up to 300 μm) containing oriented sand grains (Noffke, 2010) that appear to float in the organic matter are parallel to the layer (arrow in Fig. 9C). The close-up of this

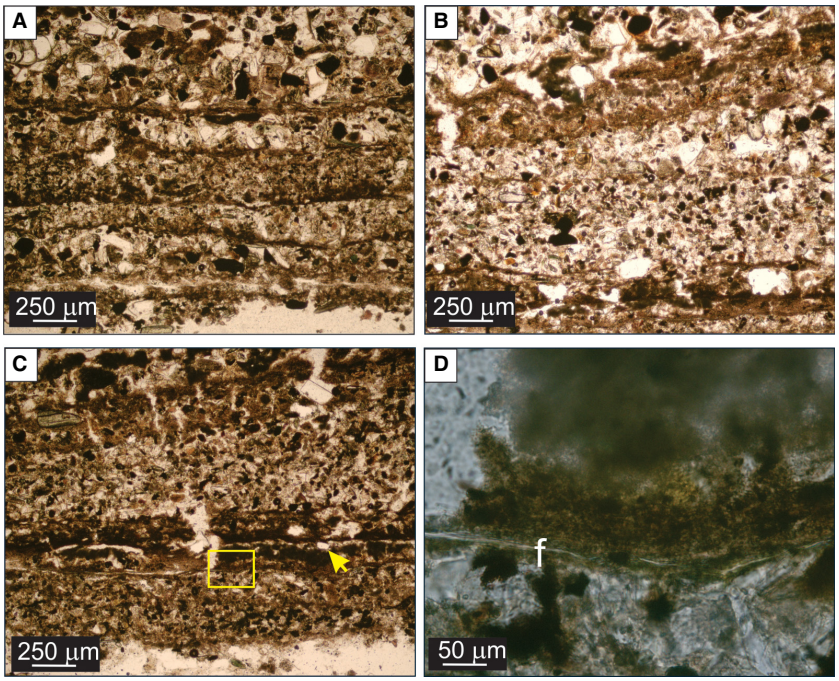

Fig. 9. Petrographic thin sections. (A) Characteristic planar lamination of microbial mats exhibiting biofilm dividing each sand layer into different grain sizes. (B) Lee face of a ripple covered by biofilm (fine sediments with organic matter) at the top and planar microbial mats at the bottom. (C) 300 μm thick biofilm at the bottom including an oriented sand grain (yellow arrow). (D) Close-up of rectangle in (C) showing a cyanobacteria filament ('f') covered by organic matter.

layer reveals the presence of brownish, cloudy organic matter (60 μm width) creating a filament-like texture (Fig. 9D), a typical characteristic of buried microbial mats (Noffke, 2000; Noffke *et al.*, 2002).

DISCUSSION

Interaction of microbially colonized sediments with hydrodynamics in a supratidal flat

The supratidal area of Paso Seco is inundated intermittently during storms when seawater enters the area behind the sand spit (Fig. 3A), as often occurs along different coasts of the world (Noffke, 2010). This is a fine example of a protected area behind a barrier where microphytobenthos (mainly diatoms and cyanobacteria) can typically colonize the siliciclastic sediments due to frequent inundation (Underwood & Paterson, 2003). Microbial cells are ubiquitous in aquatic sediments forming biofilms in siliciclastic particle surfaces (Decho, 2000) and, with continuous growth, they ultimately form flat laminated microbial mats.

Microbial mats in Paso Seco are mainly formed by filamentous cyanobacteria and diatoms, where cyanobacteria provide mechanical strength derived from the linkage of trichomes with the sediment grains, and diatoms sheltered them at the top of the surface. Both cyanobacteria and diatoms contribute to the biostabilization by an upward migration during emersion by the excretion of EPS strands (Staats *et al.*, 2000; Underwood & Paterson, 2003; Garwood *et al.*, 2015). A typical mat fabric is formed in siliciclastic sediments by the active movement of cyanobacteria and diatoms. Ultimately, sedimentary bedding reflects latency, the time span during which low or no sediment reworking takes place, enabling the microbial filaments to form a new mat fabric (binding) and to grow (Noffke, 2010). Growth includes the development of biomass by cell replication and by adhesive mucilages (EPS) being secreted. Each lamina in the microbial mat essentially represents a time frame of only minor deposition and erosion (Figs 4G, 4H, 5G and 5H), and the strands of EPS remain on mineral grain surfaces (Garwood *et al.*, 2015) producing a web of bridging strands on the sediment. Some cyanobacteria (i.e. Oscillatoria, present in the study area; Cuadrado & Pan, 2018) have filaments that glide into the polysaccharide sheath causing a new sheath (Stal, 1995). The recalcitrant structure of the sheaths and mucilage (Stal, 2001) causes the empty translucent sheaths among sand particles to remain at the bottom of the section as EPS strands between sand grains, at old microbial mats (Fig. 7F). Conversely, surface sand grains

are entangled by green filaments of living cyanobacteria forming in the freshly colonized sediment (Fig. 7C and D).

Formation and primary preservation of ripples

Normally, flooding events in Paso Seco occur under moderately energetic conditions where the inundation causes a water column height of up to 20 to 30 cm in the study zone (Fig. 3A). However, moderate to severe storms (water column >40 cm) occur when the seawater floods the narrow area with high velocities over a few hours (Fig. 3B). On these occasions, the water is >40 cm deep and of sufficiently high flow velocity to allow sand transport to occur (Fig. 4A and B). Such flood currents form different types of ripples that may be created over the microbial mats (Fig. 4D to H), in association with deformed microbially induced sedimentary structures (MISS) (Maisano *et al.*, 2019). Then, the seawater drains away slowly over the following days due to the sand spit acting as a barrier at the mouth. The weak ebb currents cause fine sediment to be deposited in the ripple troughs (arrow in Figs 4G and 5B).

Immediately after a severe storm (arrow 1 in Fig. 3B), a ripple of accumulated sand appears over a layered planar epibenthic microbial mat (Fig. 4G and H). These are 2D symmetrical wave ripples (Fig. 5B) and 3D asymmetrical current ripples (Fig. 4F). After the storm, the endobenthic microbial mats can be formed within a few hours (Noffke, 2010), due to a rapid motility of the filaments (Shepard & Sumner, 2010). In addition, the lack of water becomes sufficiently limiting on the exposed tidal flat such that a synergism between sediment dehydration and stabilization can occur (Paterson, 1989). Therefore, the ripples are stabilized during its aerial exposure (Fig. 5), showing a thin biofilm, appearing as a sticky membrane on their surface (Fig. 7A and B). These are sinoidal structures, as defined by Noffke (2010), when they are found in buried sedimentary sequences. The stabilization of ripple marks involves a rapid reorganization of microbial mat fabrics, when the sedimentation ceases, binding sedimentary particles and creating an organic layer covering a ripple mark (Figs 7A, 7B and 8A) that can be preserved in the fossil record. Likewise, grains coated by biofilms forming biotic-mineral aggregates (Noffke, 2010) that remain in suspension are ultimately deposited during calm conditions on the undulated surface, contributing to its biostabilization.

The genesis of the ripple formation described here would be similar to abiotic ripples on a sedimentary bed under a steady current, but microbial activity generates a fast means of preservation. The presence of small amounts of EPS can also increase the development time of bedforms (Malarkey *et al.*, 2015; Baas *et al.*, 2019), and even affect the type of bedforms that develop (Parsons *et al.*, 2016), because grains are inhibited from moving independently. Laboratory experiments carried out with diatom or cyanobacteria cultures also showed the importance of EPS in the transport of biostabilized sediments (Vignaga *et al.*, 2013).

Hydraulic pattern interpretation of heterolithic sedimentation under microbial mat colonization

Sinoidal structures are one type of MISS (microbially induced sedimentary structure; *sensu* Noffke *et al.*, 2001). These laminae coating the buried ripples are visible in vertical sedimentary section as laterally continuous layers forming planar and flaser beddings (Fig. 8). The interpretation of sinoidal structures contributes significantly to unravelling the biological and sedimentological relationship because they help in understanding the regular hydraulic pattern of the site. Thick lamination (millimetres to centimetres) represents a microbial mat formed under aerial exposure during latencies, when cyanobacteria respond by binding and growing. An increase in sediment transport is recorded by the sedimentary interlayers in between the sinoidal structures. Thus, the sinoidal lamination of microbial mats combined with sand layers might be interpreted as being caused by intermittent less-energetic conditions and more energetic pulses of sand transport.

Heterolithic sedimentation in a modern environment reflects the microbial interaction with gradually changing sediment dynamics (Fig. 10). A sedimentary section of 2 cm thickness shows a planar layer of fine sand (at the bottom of the section) which was deposited during three different storm events, which are each separated by the presence of very thin discontinuous organic laminae (biofilms '1' and '2' in Fig. 10B). Moreover, this sand layer displays a reduction in storm energy level from bottom to top as deduced by the decreasing sand grain size

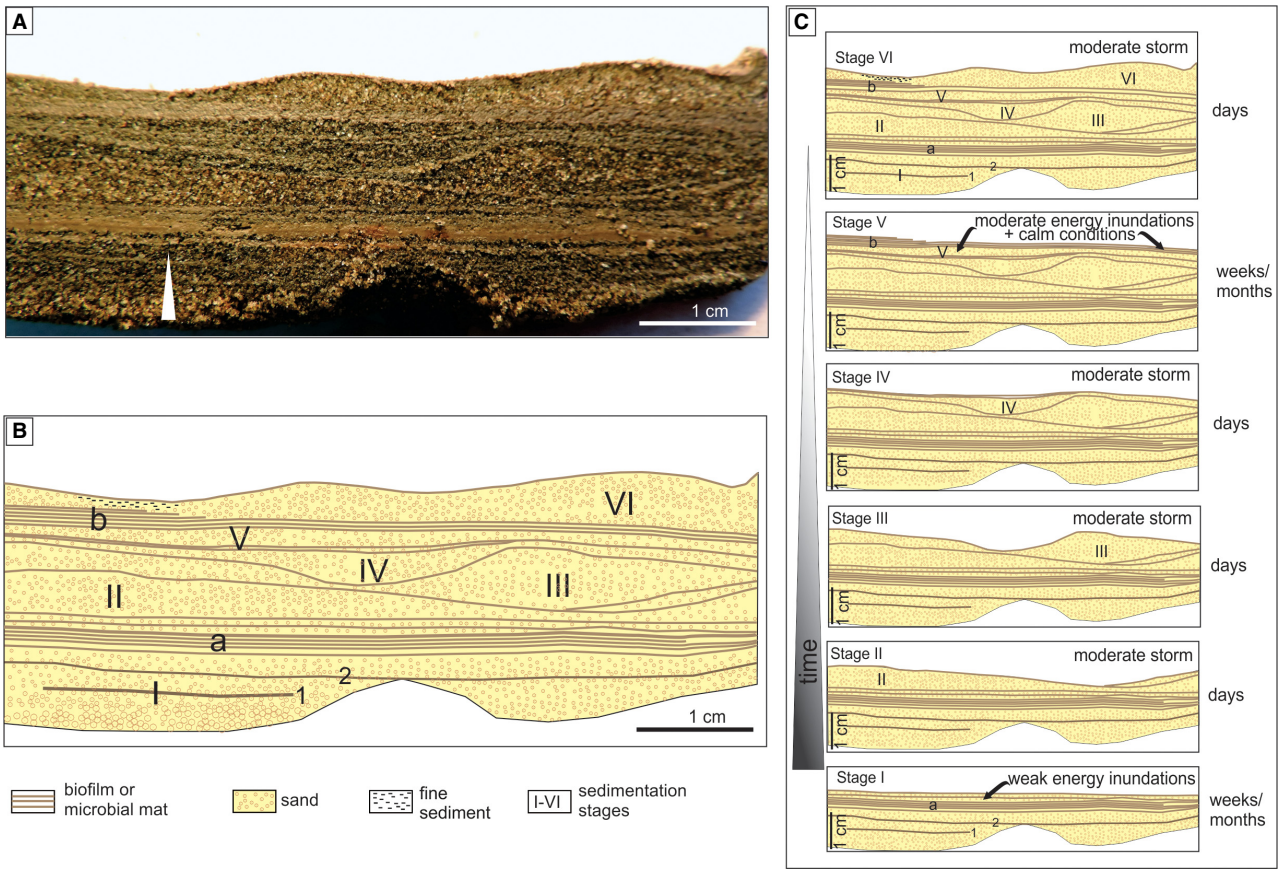

Fig. 10. Vertical sequence showing wavy bedding formed by mud layers in alternation with sand ripples, and planar lamination developed by microbial mats. The white arrow indicates diminishing sand grain size. (B) Schematic diagram showing the different stages in sedimentation (Stages I to VI, see text for details): 'a' and 'b' are micron-scale microbial mat laminae; '1' and '2' are biofilms indicating less energetic conditions and aerial exposure. (C) Individual steps of formation of heterolithic bedding shown in (B).

(white arrow in Fig. 10A). Once sedimentation ceases, cyanobacteria quickly move from beneath the microbial mat towards the new sedimentary surface (Fig. 7C and D). During latency, the sedimentary surface might be exposed for a period of weeks (or months) causing the microbial mat lamina to grow by 2 mm ('a' in Fig. 10B, Stage I in Fig. 10C) showing a planar surface. The thickness of the mat lamina (a) is correlated to the period of aerial exposure that indicates calm conditions for benthic cyanobacteria to build up microbial mats (Noffke, 2010). The top of this coherent mat is intercalated by thin sand sheets revealing inundations that transport small amounts of sand (atop 'a'). Subsequently, two more energetic events (Stages II and III, Fig. 10C) formed undulated fine-sand surfaces coated by biofilms, indicating subsequent calm conditions. The high level of storms was inferred by the formation of ripples. Stage IV contains smaller sand grains (very fine sand) refilling the trough of the previous ripples, capped with a biofilm in a relatively plane surface; inferring a less energetic storm. Sand millimetre-laminae in Stage V is also interpreted as a moderate storm (ripple formation is absent) capped with microbial mat lamina in a plane surface ('b' in Fig. 10B, Stage V in Fig. 10C). The thickness of the mat lamina is related to the duration of latency (period of aerial exposure). The sedimentary section is finished by sand accumulation forming ripples (Stage VI in Fig. 10C) as a consequence of a severe storm. Finally the ripples are capped by a thin biofilm formed during calm conditions (tidal flat aerial exposure).

A heterolithic sequence comprising two different sand-layers (laminar and undulated) shows different levels of storm-energy (Fig. 11). A severe storm is inferred from undulating sand

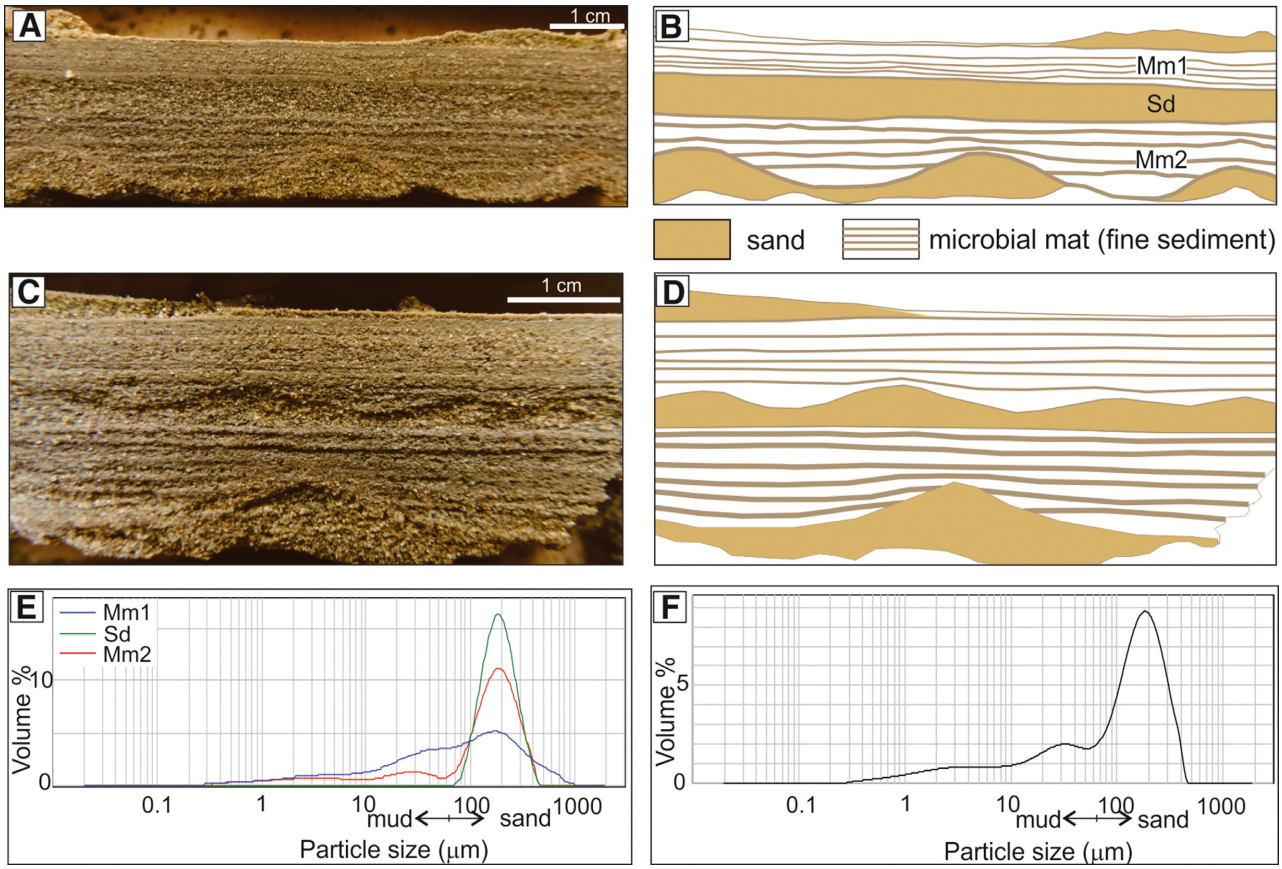

Fig. 11. Vertical sedimentary section in response to changing hydrodynamic conditions. (A) Energetic (sand ripple formation) and moderate hydrodynamic events (sand layer) followed by microbial mat formation (less energetic conditions). (B) Schematic diagram of (A). Mm: microbial mat laminae. Sd: sand layer. (C) Two events of energetic conditions (sand ripple formation) followed by microbial mat formation (less energetic conditions). (D) Schematic diagram of (C). (E) Grain-size analysis of microbial mat laminae (Mm1 and Mm2) and sand layers (Sd) shown in (B). (F) Grain-size analysis of the mixture of Mm1 + Sd + Mm2, shown in (B). See text for details.

bedding, and a moderate storm is inferred by laminar sand bedding, each capped by microbial mats formed during calm conditions (Mm1 and Mm2 in Fig. 11B). Two severe storm events (undulated sand-layers) were assumed in Fig. 11C followed by calm conditions.

The ripples documented here can be compared with experimental research under combined flows. Perillo *et al.* (2014) defined an upper-stage plane bed (USPB) generated by intense sediment movement layer of 1 cm in thickness under a combined flow from unidirectional and oscillatory flows. These conditions may be comparable with moderate storms in the study zone creating planar sand layers without ripple formation (Fig. 11). Moreover, severe storms may create 3D asymmetrical ripples (Fig. 4H) under combined flow by weak oscillatory velocities (<0.15 m s^{-1}, measured by Perillo *et al.*, 2014) and relative strong unidirectional flows (>0.2 m s^{-1}) due to current amplification in the narrow study area.

It is essential to emphasize that there is a difference in the temporal scale between the mat and sand layers: the sand layer takes one to two days (the duration of a storm) to form; and the microbial mats can take several weeks or months (the latency period between storms or inundations) to form. The coarse sediments represent oxic environments (Fig. 6) with low organic material preservation potential, but high EPS/microalgae content that can enhance the potential for ripple preservation (Friend *et al.*, 2008). In contrast, the fine sediments are anoxic layers due to the bacterial content. This is the reason why the sand layers easily disjoint under dry conditions and the fine sediments maintained their integrity (Fig. 6C).

Mixed sand–mud depositional environment

Grain-size analyses commonly involve samples from the top few centimetres of the surface including sand ripples *ca* 10 to 20 mm below the base of the ripple. A vertical profile of the tidal flat of the study area shows that the bulk sediment between the crest and base of the ripple and down 20 mm below the base comprised from the top: biofilm, sand (body of the ripple) and microbial mat (Figs 4G, 4H, 5D, 6A, 7, 8, 10 and 11). In fact, the grain-size analyses for each layer in the first 2 cm of the sedimentary surface of Fig. 11A reveals that the surficial microbial mat (Mm2, Fig. 11B) is composed mainly of a mixture of sand and mud by grain-size analysis (Fig. 11E). The underlying sedimentary layer is composed of only fine sand (Sd, Fig. 11E), and the lower microbial mat layer (Mm1) shows a bimodal size distribution composed mainly by fine sand and mud (Mm2, Fig. 11E), due to the <1 mm thick sand laminae incorporated in the mat. However, the three layers grouped together (the whole 2 cm surficial sediment) show a bimodal size distribution (peaks in fine sand and coarse silt) of mixed sand–mud composition with 31.33% of mud by volume (Fig. 11F). So, microbial mats may be misinterpreted as mud.

It is important to establish whether the mixed sand–mud sediment is derived from thin millimetre to centimetre-scale lamination, because this would lead one to suspect that the sediment was colonized by biota and therefore that each layer was developed under a different hydrodynamic regime. Because bedforms are essential predictors of palaeoenvironmental reconstruction, the interpretation in the geological record should take into consideration the important effect that colonized sediments have on the preservation of ripples. Recognition of biostabilized ripples is essential to a proper palaeointerpretation. The first clue to identifying ripples preserved by microbial activity is the characteristic lamination of the microbial mats where they rest, and the sinoidal structure covering them.

CONCLUSIONS

Paso Seco provides a better understanding of processes occurring as a result of a seaward coastal progradation. The transitional zone between the continental and marine environments is characterized by intermittent flooding events with varying hydrodynamic intensity that alternate with sufficiently quiescent conditions to allow microbial sediment colonization. This study reveals the importance that biological factors have in coastal sedimentation sustained by microbial mats acting as a good indicator of the hydraulic conditions that govern the area. Moreover, sediment transport creates laminar sand bedding or small two-dimensional and three-dimensional ripples, depending on the intensity of the storms.

The proposed geobiological model assists in the interpretation of heterolithic sedimentary sections, where the ripples are biostabilized by microbial activity. The model was obtained through a detailed inspection of sedimentary sections, on scales comparable to the dimensions of the microbial world. Less energetic conditions and tidal flat exposure create planar lamination of microbial mats; more energetic conditions create millimetre-thick sand layers over microbial mats; and the most energetic conditions under unidirectional currents create 3D ripples, associated with energetic sediment transport and erosional microbially induced sedimentary structures (MISS). The biological activity in response to hydrodynamics preserves the ripples or sand layers by micro-organism motility and their rapid excretion of Extracellular Polymeric Substances. The clue to recognition of biostabilized ripples in a sedimentary record is the characteristic lamination of the microbial mats where they rest, and the sinoidal structure covering them, that commonly might be misinterpreted as fine sediment. The identification of microbial activity in sediment stabilization minimizes a biased palaeoenvironmental interpretation.

ACKNOWLEDGEMENTS

This research was supported by CONICET (grant PIP 2013 No. 4061) and SECYT-UNS (grant PGI 24/H138). Thanks to L. Maisano, V.L. Perillo, E.A. Gómez, I.E. Quijada, L.A. Raniolo for their assistance in the field work, and H. Pellegrini for the grain-size analyses. I am grateful to N. Scivetti from Laboratorio de Petronomia (Universidad Nacional del Sur) who made the petrographic thin sections. I also thank J. Malarkey and N. Noffke, as well as Associate Editor J. Baas, for their valuable suggestions to improve an earlier version of this paper.

REFERENCES

Baas, J.H., **Baker, M.L.**, **Malarkey, J.**, **Bass, S.J.**, **Manning, A.J.**, **Hope, J.A.**, **Peakall, J.**, **Lichtman, I.D.**, **Ye, L.**, **Davies, A.G.**, **Parsons, D.R.**, **Paterson, D.M.** and **Thorne, P.D.** (2019) Integrating field and laboratory approaches for ripple development in mixed sand-clay-EPS. *Sedimentology*, **66**, 2749–2768.

Cuadrado, D.G. and **Blasi, A.** (2017) Presencia de actividad microbiana en ambientes silicoclásticos actuales y en paleoambientes. Estudio comparativo para el establecimiento de análogos. *Latin Am. J. Sedimentol. Basin Anal.*, **24**, 39–73.

Cuadrado, D.G. and **Pan, J.** (2018) Field observations on the evolution of reticulate patterns in microbial mats in a modern siliciclastic coastal environment. *J. Sed. Res.*, **88**, 24–37.

Cuadrado, D.G., **Perillo, G.M.E.** and **Vitale, A.** (2014) Modern microbial mats in siliciclastic tidal flats: evolution, structure and the role of hydrodynamics. *Mar. Geol.*, **352**, 367–380.

Cuadrado, D.G., **Pan, J.**, **Gómez, E.A.** and **Maisano, L.** (2015) Deformed microbial mat structures in a semiarid temperate coastal setting. *Sed. Geol.*, **325**, 106–118.

Dalrymple, R.W., **Mackay, D.A.**, **Ichaso, A.A.** and **Choi, K.S.** (2012) Processes, morphodynamics, and facies of tide-dominated estuaries. In: *Principles of Tidal Sedimentology* (Eds Davis, R.A. Jr and Dalrymple, R.), pp. 79–107. Springer, Dordrecht.

Davies, R.A. Jr (2012) Tidal signatures and their preservation potential in stratigraphic sequences. In: *Principles of Tidal Sedimentology* (Eds Davis, R.A. Jr and Dalrymple, R.), pp. 35–55. Springer, Dordrecht.

Decho, L.W. (2000) Microbial biofilms in intertidal systems: an overview. *Cont. Shelf Res.*, **20**, 1257–1273.

Eisma, D. (1986) Flocculation and de-flocculation of suspended matter in estuaries. *J. Sea Res.*, **20**, 183–199.

Friend, P.L., **Lucas, C.H.**, **Holligan, P.M.** and **Collins, M.B.** (2008) Microalgal mediation of ripple mobility. *Geobiology*, **6**, 70–82.

Garwood, J.C., **Hill, P.S.**, **MacIntyre, H.L.** and **Law, B.A.** (2015) Grain sizes retained by diatom biofilms during erosion on tidal flats linked to bed sediment texture. *Cont. Shelf Res.*, **104**, 37–44.

Gehling, J. (1999) Microbial mats in terminal Proterozoic siliciclastics: Ediacaran death masks. *Palaios*, **14**, 40–57.

Maisano, L., **Cuadrado, D.G.** and **Gómez, E.A.** (2019) Processes of MISS-formation in a modern siliciclastic tidal flat, Patagonia (Argentina). *Sed. Geol.*, **381**, 1–12.

Malarkey, J., **Baas, J.H.**, **Hope, J.A.**, **Aspden, R.J.**, **Parsons, D.R.**, **Peakall, J.**, **Paterson, D.M.**, **Schindler, R.J.**, **Ye, L.**, **Lichtman, I.D.**, **Bass, S.J.**, **Davies, A.G.**, **Manning, A.J.** and **Thorne, P.D.** (2015) The pervasive role of biological cohesion in bedform development. *Nat. Commun.*, **6**, 6257.

Martin, A.J. (2000) Flaser and wavy bedding in ephemeral streams: a modern and an ancient example. *Sed. Geol.*, **136**, 1–5.

Neumann, A., **Gebelein, C.** and **Scoffin, T.** (1970) The composition, structure and erodability of subtidal mats, Abaco, Bahamas. *J. Sed. Petrol.*, **40**, 274–297.

Noffke, N. (2000) Extensive microbial mats and their influences on the erosional and depositional dynamics of a siliciclastic cold water environment (Lower Arenigian, Montagne Noire, France). *Sed. Geol.*, **136**, 207–215.

Noffke, N. (2010) *Microbial Mats in Sandy Deposits from the Archean Era to Today*. Springer- Verlag, Berlin, 194 pp.

Noffke, N., **Gerdes, G.**, **Klenke, T.** and **Krumbein, W.E.** (2001) Microbially induced sedimentary structures: a new category within the classification of primary sedimentary structures. *J. Sed. Res.*, **71**, 649–656.

Noffke, N., **Knoll, A.H.** and **Grotzinger, J.P.** (2002) Sedimentary controls on the formation and preservation of microbial mats in siliciclastic deposits: a case study from the Upper Neoproterozoic Nama Group, Namibia. *Palaios*, **17**, 533–544.

Parsons, D.R., **Schindler, R.J.**, **Ye, L.**, **Simmons, S.**, **Hope, J.A.**, **Malarkey, J.**, **Baas, J.H.**, **Peakall, J.**, **Manning, A.J.**, **Leiping, Y.**, **Paterson, D.M.**, **Aspden, R.J.**, **Bass, S.J.**, **Davies, A.G.**, **Lichtman, I.D.** and **Thorne, P.D.** (2016) The role of biophysical cohesion on subaqueous bed form size. *Geophys. Res. Lett.*, **43**, 1566–1573.

Paterson, D. (1989) Short-term changes in the erodibility of intertidal cohesive sediments related to the migratory behavior of epipelic diatoms. *Limnol. Oceanogr.*, **34**, 223–234.

Paterson, D. (1994) Microbial mediation of sediment structure and behaviour. In: *Microbial Mats* (Eds Stal, L. and Caumette, P.), Ecological studies, **35**, 97–109. Springer, Berlin, Heidelberg, New York.

Perillo, M.M., **Best, J.L.** and **Garcia, M.H.** (2014) A new phase diagram for combined-flow bedforms. *J. Sed. Res*, **84**, 301–313.

Perillo, V.L., **Maisano, L.**, **Martinez, A.M.**, **Quijada, I.E.** and **Cuadrado, D.G.** (2019) Microbial mat contribution to the formation of an evaporitic environment in a temperate-latitude ecosystem. *J. Hydrol.*, **575**, 105–114.

Reineck, H.E. and **Wunderlich, F.** (1968) Classification and origin of flaser and lenticular bedding. *Sedimentology*, **11**, 99–104.

Shepard, R.N. and **Sumner, D.Y.** (2010) Undirected motility of filamentous cyanobacteria produces reticulate mats. *Geobiology*, **8**, 179–190.

Staats, N., **Stal, L.J.**, **de Winder, B.** and **Mur, L.R.** (2000) Oxygenic photosynthesis as driving process in exopolysaccharide production of benthic diatoms. *Mar. Ecol. Prog. Ser.*, **193**, 261–269.

Stal, L.J. (1995) Physiological ecology of cyanobacteria in microbial mats and other communities. *New Phytol.*, **131**, 1–32.

Stal, L.J. (2001) Coastal microbial mats: the physiology of a small-scale ecosystem. *S. Afr. J. Bot.*, **67**, 399–410.

Stal, L.J. (2003) Microphytobenthos, their extracellular polymeric substances, and the morphogenesis of intertidal sediments. *Geomicrobiol. J.*, **20**, 463–478.

Stal, L.J. (2013) In: Cyanobacterial mats and stromatolites. In: *Ecology of Cyanobacteria II: Their Diversity in Space and Time* (Ed. Whitton, B.A.), pp. 65–125. Springer, Dordrecht.

Steel, R.J., **Plink-Bjorklund, P.** and **Aschoff, J.** (2012) Tidal deposits of the Campanian Western Interior Seaway, Wyoming, Utah and Colorado, USA. In: *Principles of Tidal Sedimentology* (Eds Davis, R.A. Jr and Dalrymple, R.W.), pp. 437–471. Elsevier, Dordrecht.

Terwindt, J.H.J. and **Breusers, H.N.C.** (1982) Flume experiments on the origin of flaser bedding. *Sedimentology*, **29**, 903–907.

Trebino, L.G. (1987) Geomorfología y evolución de la costa en los alrededores del pueblo de San Blas, provincia de Buenos Aires. *Rev. Asoc. Geol. Argentina*, **42**, 9–22.

Underwood, G.J.C. and **Paterson, D.M.** (2003) The importance of extracellular carbohydrate production by marine epipelic diatoms. *Adv. Bot. Res.*, **40**, 183–240.

Vignaga, E., **Sloan, D.M.**, **Luo, X.**, **Haynes, H.**, **Phoenix, V.R.** and **Sloan, W.T.** (2013) Erosion of biofilm-bound fluvial sediments. *Nature Geosci.*, **6**, 770–774.

Virolle, M., **Brigaud, B.**, **Bourillot, R.**, **Fenies, H.**, **Portier, E.**, **Duteil, T.**, **Nouet, J.**, **Patrier, P.** and **Beaufort, D.** (2018) Detrital clay grain coats in estuarine clastic deposits: origin and spatial distribution within a modern sedimentary system, the Gironde Estuary (south-west France). *Sedimentology*, **66**, 859–894.

Wang, P. (2012) Principles of sediment transport applicable in tidal environments. In: *Principles of Tidal Sedimentology* (Eds Davis, R.A. Jr and Dalrymple, R.W.), pp. 19–33. Springer, Dordrecht.

Wooldridge, L.J., **Worden, R.H.**, **Griffiths, J.**, **Thompson, A.** and **Chung, P.** (2017) Biofilm origin of clay-coated sand grains. *Geology*, **45**, 875–878.

Manuscript received 23 October 2019; revision accepted 4 February 2020